

# Comparison between geometrically focused pulses versus filaments in femtosecond laser ablation of steel and titanium alloys

Anthony Valenzuela · Chase Munson ·  
Andrew Porwitzky · Matthew Weidman ·  
Martin Richardson

Received: 13 February 2013 / Accepted: 4 November 2013  
© Springer (outside the USA) 2013

**Abstract** Kerr self-focusing of high-power ultrashort laser pulses in atmosphere may result in a structure or structures of high intensity that can propagate over long distances with little divergence. Filamentation has garnered significant interest in the nonlinear optics community due to its unique properties. Salient features of filaments include a central region of intense laser power (greater than the ionization threshold of the propagation medium) and a low temperature plasma column that lasts up to nanoseconds in duration after the passage of the laser pulse. Steel and titanium samples are ablated by filaments and by sharply focused sub-picosecond laser pulses. We then performed metrology on the samples to compare the ablation features in addition to modeling of the plasma ablation process. Ablation with filaments leads to a wider range of material responses as compared to ablation with sharply focused pulse. This results in potential complications for applications of filament ablation that depends on the rate of material removal and spectroscopic analysis.

## 1 Introduction

With the advent of nonlinear optics and the method of chirped pulse amplification, we are able to expose matter to extremely intense bursts of laser light. Of particular note in

the field of nonlinear optics is filament propagation in atmosphere, spawning a wide array of studies (see review articles in [1–3]). The filamentation process takes advantage of air molecules that would disrupt laser propagation linearly, however, in the case of an intense sub-picosecond laser pulse can act in a nonlinear manner. For example, a 1 mJ collimated laser pulse with a pulse duration of 100 fs (10 GW) can experience Kerr self-focusing that will create an increase in intensity beyond the ionization threshold of air (greater than  $10^{12}$  W/cm<sup>2</sup>). The resultant plasma core defocuses the laser light, and under the proper conditions, the competing processes create a filament structure that can exist for hundreds of meters [4].

The filament structure consists of a plasma column of approximately 100  $\mu$ m in diameter [5, 6] surrounded by an energy reservoir as shown in Fig. 1. Of the initial laser energy, at least half is needed in the reservoir to sustain the intense core that results in a plasma column [7]. The energy reservoir exists on the same timescale as the initial laser pulse (sub-picosecond); however, the plasma column takes much longer to dissipate the energy stored in both the free electrons and ions. Thermalization of the approximately 1 eV electrons happens well after the laser pulse has passed, and the recombination time is on the order of nanoseconds or less [8].

Using focused ultrashort pulse lasers (USPL) for ablation is attractive due to the precise manner in which material is removed. A recent review of USPL ablation as applied to micromachining is given by Cheng et al. [9]. The hallmark of this process is a clean crater with minimal spall on the target, whereas nanosecond (and longer) pulses will leave a ragged crater and material strewn along the surface [10]. This arises from rapid transition of solid target material to a liquid phase via superheating during the laser pulse [11, 12]. Work done by Kiselev et al. [13]

---

A. Valenzuela (✉) · C. Munson · A. Porwitzky  
U.S. Army Research Laboratory,  
Aberdeen Proving Ground, MD 21005, USA  
e-mail: anthony.r.valenzuela6.civ@mail.mil

M. Weidman · M. Richardson  
Townes Laser Institute and CREOL, The College of Optics  
and Photonics, University of Central Florida, Orlando,  
FL 32816, USA

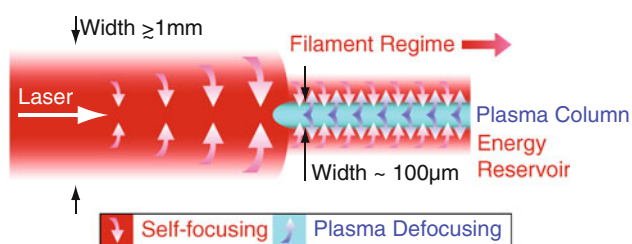


**Fig. 1** Sketch of laser propagation in which Kerr self-focusing and competitive plasma defocusing leads to the production of a filament

demonstrates the inherent benefits of the concentrated ultrashort energy in the filament structure to ablate and cut through solid matter, termed Filament-Induced Laser Machining (FILM). As opposed to complex three-dimensional machining by mechanically moving the focusing lens or target, a filament is able to ablate and cut along a much larger depth versus the Rayleigh range. The microscopic properties of filament ablation such as diameter and volume removed show less than 30 and 50 % relative standard deviation, respectively, in the absence of geometric focusing over distances up to 50 m [14]. Related to FILM is the concept of filament-induced breakdown spectroscopy (FIBS), essentially utilizing a filament to interrogate the chemical make up of a target or a coating on a target in the manner of laser-induced breakdown spectroscopy [15, 16] (LIBS) but at remote distances [17–19]. In our study of how the focal and nonlinear optical conditions impact the ablation process, we have defined three regimes: Sharply Focused Femtosecond Laser Machining (SFFLM), Assisted Filament-Induced Laser Machining (AFILM), and Lensless Filament-Induced Laser Machining (LFILM). SFFLM is achieved using what we consider a short focal length lens that reduces the possible filamentation regime to nearly the Rayleigh range. AFILM uses a long focal length lens in addition to self-focusing to generate a filament ahead of the geometric focus; the filament extends for much longer than the Rayleigh range. Finally, LFILM does not use a lens but relies on self-focusing to generate a filament.

## 2 Experimental Setup

For the experiment, all three regimes were achieved using the same USPL system but with different focusing principles as shown in Fig. 2. Our laser produces pulse energies of up to 25 mJ in 100 fs pulsewidth at 800 nm center wavelength with an initial beam size of approximately 1 cm in diameter. The SFFLM regime was created by using a  $f_s = 25\text{cm}$  lens (similar to conventional ablation studies) and the AFILM regime using a  $f_l = 2\text{ m}$  lens. The targets were placed before, at, and after the focal point for both

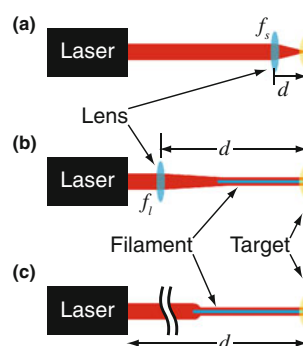


**Fig. 2** Experimental setup showing the three regimes: **a** Fast focus, SFFLM; **b** Slow focus forming a filament, AFILM; and **c** collimated (no optical lens) forming a filament, LFILM

SFFLM and AFILM; the positions before and after the focal point have approximately the same intensity given a linear Gaussian focus. The primary method we used for controlling the self-focusing of the collimated beam in LFILM was by changing the frequency chirp from the laser compressor. As such, we were able to achieve strong self-focusing in the LFILM regime as close as 3 m from the end of the compressor.

A distinguishing aspect of the filament structure is the long region of intense power (necessarily greater than the ionization threshold of the medium) that can exist for many meters, far in excess of the Rayleigh range. To examine how that is manifested in the ablation phenomenon, the target was placed before, at, and after the focus position for the SFFLM and AFILM cases. Those distances,  $d$  as shown in Fig. 2, were measured from the lens. In LFILM, the target was placed at positions before, immediately after, and well after the position where self-focusing is pronounced. Those distances,  $d$ , were measured relative to the end of the laser system.

For each ablation point, the target materials were exposed to 1, 10, or 25 successive pulses (1 to 2 Hz repetition rate, approximately 10 mJ giving 100 GW peak power) to examine cumulative effects. The materials chosen were all visually opaque, without any special coatings, and are listed in Table 1 along with selected material properties. The sample surfaces were prepared by grinding to a finish of approximately  $3\ \mu\text{m}$  peak-to-valley for the steels and  $6\ \mu\text{m}$  for bulk titanium. The samples were then examined using a white-light interferometer (Newview 6300, Zygo Corp.) to obtain surface profile data. The root-mean-square (rms) variation in the sample surface height as measured by the interferometer was  $0.06\ \mu\text{m}$  for the steel samples and  $0.30\ \mu\text{m}$  for bulk titanium. In order to more closely examine the shot-to-shot variations in ablation, we utilized a smooth titanium sample. These samples were electron beam vapor deposited with a thickness of  $1\ \mu\text{m}$  on sapphire substrate to a rms roughness of approximately

**Table 1** Selected properties of target materials at 298 K [20–23]

Material	Main composition	Thermal conductivity (W/cm K)	Absorption coefficient at 800 nm ( $\mu\text{m}^{-1}$ )
Low carbon steel 1018	98.5–99.1 % Fe	0.803	57.2
Stainless steel 304	62.5–74 % Fe, 18–20 % Cr, 8–12 % Ni	0.163	47.0
Titanium (bulk and smooth)	>99.0 % Ti	0.22	52.1

0.01  $\mu\text{m}$  and placed at a distance of 11.8 m from the laser for LFILM.

### 3 Results

The ablation results show a sharp contrast between the short focus regime (SFFLM) and the two filamented regimes (AFILM and LFILM) in the ability to remove material. Figure 3 displays the results from the low carbon steel target and is qualitatively representative of the results seen in stainless steel and bulk titanium (not shown). In Fig. 3a, the SFFLM process leads to a sharp crater when the target is placed at the focal point of the 25 cm lens. At the SFFLM focal point, the Gaussian intensity,  $I$ , approaches  $2 \times 10^{16} \text{W}/\text{cm}^2$ . This creates a well-defined crater

approximately 200  $\mu\text{m}$  wide (about 5 times the spot size) and a lip with a peak-to-valley height difference of about 5  $\mu\text{m}$  with approximately  $5 \times 10^{-5} \text{mm}^3$  (0.39  $\mu\text{g}$ ) of material removed. In this sharply focusing regime, the laser intensity surpasses the ionization threshold of air, on the order of  $10^{12} - 10^{13} \text{W}/\text{cm}^2$ , leading to breakdown; this region extends 3 cm on either side of the focal point. However, we can see from the average cross sections (over 11 lines of data) in Fig. 4a that placing the target 6 cm on either side of the focal point ( $d = 19 \text{cm}$  or  $31 \text{cm}$ , spot size of 2.1 mm,  $I = 6.4 \times 10^{11} \text{W}/\text{cm}^2$ ) results in little ablation. Similar results are seen in stainless steel (Fig. 4b) and bulk titanium (Fig. 4c).

Switching to the AFILM regime with a 2-m focal length lens, it produces a marked change in the ablation results. As shown in Figs. 3b and 5a, a less-defined crater is seen on low carbon steel at the focal point though the affected area is almost twice as wide. The depth in the center of ablation area is shallower than in SFFLM though this results in roughly the same volume of material removed. This is despite the peak intensity being almost two orders of magnitude less. Similarly, the stainless steel target in Figs. 5b and 6 shows a clear deviation from a circular feature in the ablated area at 2 and 2.47 m from the lens though the spot size and intensity are similar to the 19 and 31 cm positions in SFFLM (Fig. 4a), demonstrating that we are in a nonlinear optical regime. This structure may be the result of the laser pulse entering the multiple filament regime where individual filaments can form from the initial

**Fig. 3** False color height data of low carbon steel target after 25 pulses with **a** SFFLM  $f_s = 25 \text{ cm}$  at  $d = 25 \text{ cm}$ , **b** AFILM  $f_s = 2 \text{ m}$  at  $d = 2 \text{ m}$ , and **c** LFILM at  $d = 10.4 \text{ m}$

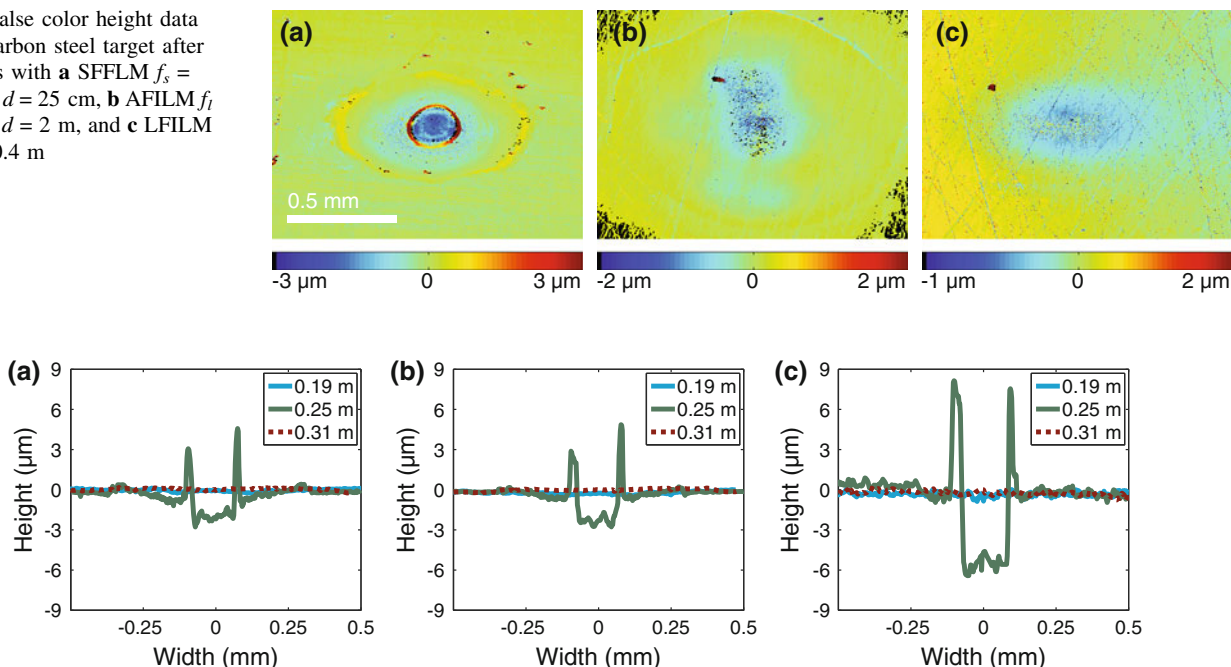


**Fig. 4** Average cross section of low carbon steel (a), stainless steel (b), and bulk titanium (c) targets along the direction of laser polarization after 25 pulses, with SFFLM  $f_s = 25 \text{ cm}$ . Colored lines denote different target distances,  $d$ , relative to the lens

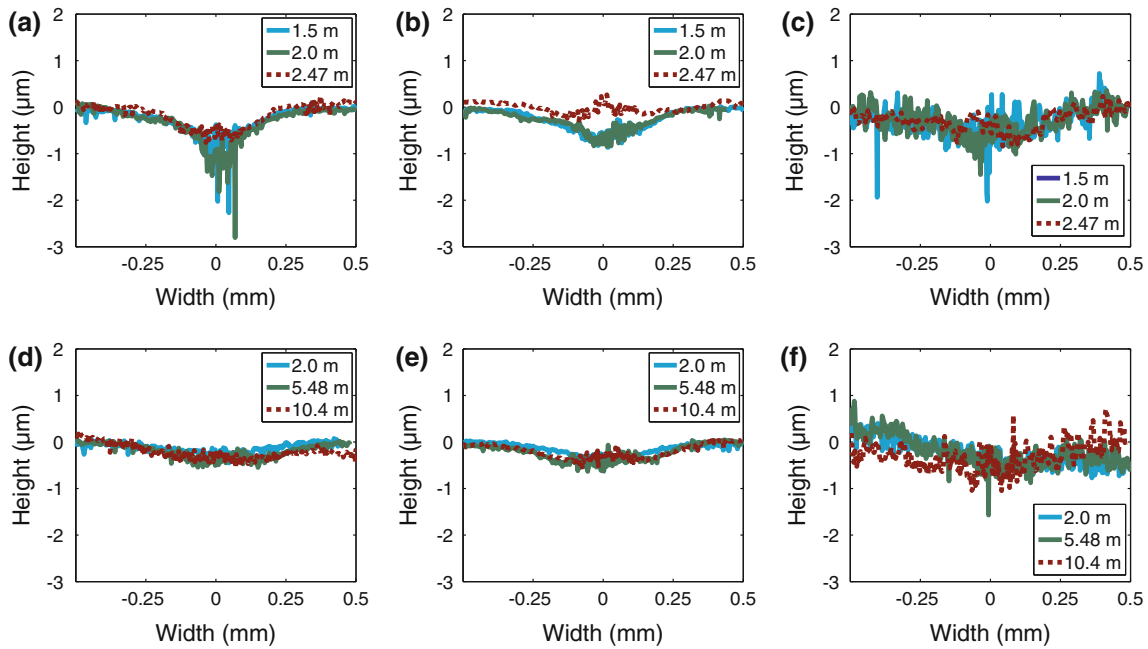


**Fig. 5** Average cross section of low carbon steel (a, d), stainless steel (b, e), and bulk titanium (c, f) targets along the direction of laser polarization after 25 pulses, with (a–c) AFILM  $f_l = 2$  m; and

(d–f) LFILM, no lens. Colored lines denote different target distances,  $d$ , relative to the lens (a–c) or laser system (d–f)

**Fig. 6** False color height data for stainless steel target after 25 pulses with AFILM  $f_l = 2$  m at a  $d = 1.5$  m, b  $d = 2$  m, and c  $d = 2.47$  m from the lens. Scales are identical for each image

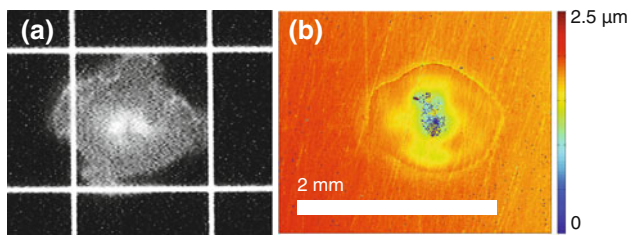
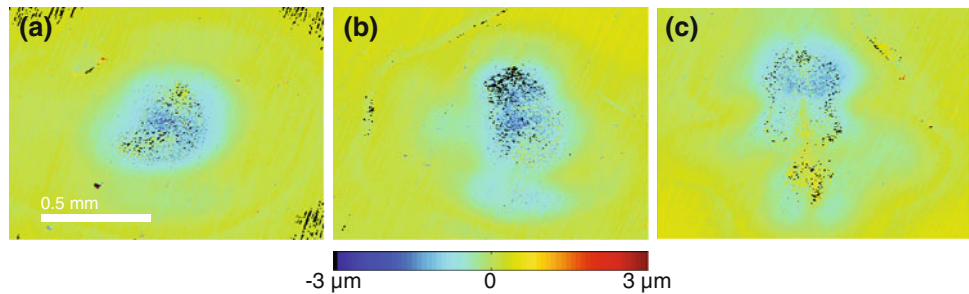


**Fig. 7** AFILM comparison at focal point ( $d = 2$  m) of a single pulse burn paper (white 2 mm grid lines), and b 25 pulses on low carbon steel

pulse [24–26]. At the peak power of our pulse (100 GW), we could expect up to 10 individual filaments to form [27]. However, we observe on burn paper (Fig. 7a) a non-circular area that may result from multiple filaments that would correspond to the complex ablation pattern seen in Fig. 7b. It is important to note the sharp topographic variation between Fig. 6a and c despite being almost

equidistant from the focus demonstrating a substantial change to the profile of the laser pulse. However, the peak-to-valley surface height varies little at the different values of  $d$ , in comparison with that seen in SFFLM (see Fig. 5a–c). The bulk titanium target showed less susceptibility to material removal at any distance under AFILM, but rather showed a pronounced visual change to the surface (i.e., darkening). This result is in sharp contrast to the observed SFFLM ablation material removal and crater depth in Fig. 4c when compared to the steel targets.

Removing the lens and adjusting the frequency chirp, we then created a filament based on self-focusing without geometric focusing. In this LFILM regime, we start to see strong self-focusing at 3 m from the end of the laser system and strong continuum generation by 5 m. Figure 3c shows an ablation area on low carbon steel that is not as sharply defined as in the SFFLM (Fig. 3a) and AFILM (Fig. 3b) regimes even at 10.4 m from the laser. The ablation area is even larger than SFFLM and AFILM, possibly due to



higher pointing instability from a lack of geometrical focusing, with the ablation depth less and only about half the volume of material removed. The remarkable result of LFILM is the reproducibility of the ablation features of the steel targets over a wide variation in  $d$  as shown in Fig. 5d, e. As in the AFILM case for the steels, the bulk titanium target seen in Fig. 8 was much less affected by LFILM in terms of ablation and material removal, however, showed a significant darkening of the surface [28, 29].

We examined the smooth titanium targets in LFILM and see in Fig. 9a a crater size of approximately 0.5 mm in diameter in agreement with the bulk substrate target (Fig. 8). A central peak of material rises above the ablation crater floor in the single ablation spot in Fig 9a, and the maximum transverse beam movement can be measured by quantifying the distance between peaks produced by two or more sequential laser pulses. In this example, the peak-to-peak distance is less than 0.4 mm (Fig 9b). We expect the most variation in transverse beam movement in LFILM due to a lack of geometrical focusing. As can be seen in Fig 9b, the movement of the laser pulse can have both parallel and perpendicular motion relative to the laser polarization (in this figure vertical). Increasing the number of pulses results in a preferential elliptical region of ablation of approximately 0.78 mm diameter parallel to the laser polarization direction and 0.63 mm diameter

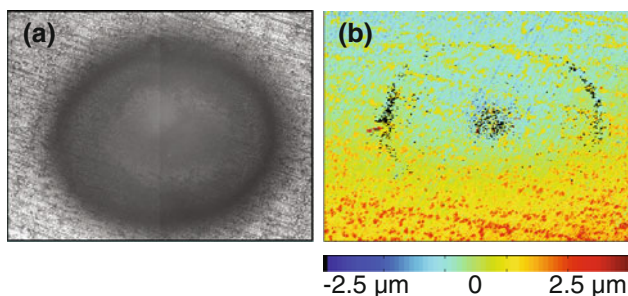


**Fig. 8** LFILM of bulk titanium target at  $d = 10.4$  m after 25 pulses: **a** raw monochrome image and **b** false color height data

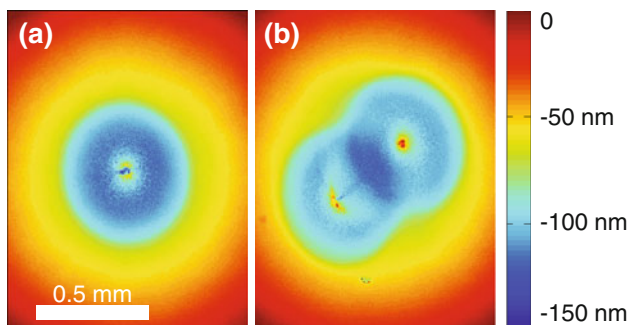


**Fig. 9** Smooth titanium target after **a** 1 pulse and **b** 2 pulses LFILM at  $d = 11.8$  m from the laser system, false color height data

perpendicular after 100 pulses (data not shown). Examining the detectable peak-to-peak movement, the average over all the samples was 0.21 mm with a standard deviation of 0.13 mm.

#### 4 Plasma ablation simulations

In order to understand the ablative properties of the plasma component of the filament in FILM, a plasma ablation model was developed to represent the possible effect the lingering plasma column may have on the target surface. The plasma ablation model used here has successfully modeled atmospheric ablation of pulsed plasma thrusters, plasma-propellant interactions, and arc discharges and is fully detailed in [30]. The model is based on the concept of coupling Anisimov’s vacuum laser ablation theory to a hydrodynamic, non-equilibrium layer to relate the target properties to the bulk plasma properties [31]. In order to close the model’s system of equations, the vapor pressure of the target is required. A Clausius–Clapeyron relation was fitted using data from room temperature [32], having found that the final temperature of the target does not change significantly. Finally, the model consists of solving a single algebraic equation numerically to determine the ablation rate of the target.

The ablation rate is dependent on the instantaneous surface temperature of the target and may change with time. Thus, the ablation model (detailed description given in Chapter 4 of Ref. [30]) was coupled to an axisymmetric two-dimensional thermal conduction model to represent the target depth (see Fig. 10). A finite plasma column radius of 50  $\mu\text{m}$  was assumed, while the computational

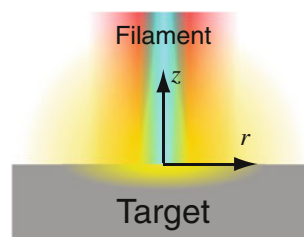


**Fig. 10** Simulation layout used with filament impinging on metal target in axisymmetric model

**Table 2** List of material properties at 298 K and 1 atm used in simulations [20, 21]

Material	Density $\text{g/cm}^{-3}$	Specific Heat at Constant Pressure $\text{J/kg K}$	Heat of Vaporization $\text{J/kg}$
Iron	7.86	450	$6.09 \times 10^6$
Titanium	4.51	523	$8.88 \times 10^6$

domain had a radial extent of five times the column radius. Target depth was half the radial extent making it functionally semi-infinite for the timescales considered here. The thermal model requires thermodynamic properties (see Table 2) for the target such as thermal diffusivity, heat of vaporization, and density. For temperature dependent values, room temperature data was used.

Some assumptions on the state of the plasma column had to be made due to lack of experimental data probing the filament. Total heat flux reaching the target, bulk plasma number density, and bulk plasma temperature are required inputs to the model. For these parameters, values from typical atmospheric density plasma ablation were used and were selected to yield the greatest calculated target ablation. These parameters are  $10^5 \text{W/cm}^2$ ,  $10^{15} \text{cm}^{-3}$ , and 1.5 eV, respectively. Targets simulated were titanium and iron (similar in composition to the low carbon steel target material).

Based on known properties of filaments, it was assumed that the plasma column will only persist in the atmosphere for 1 ns after the laser pulse. Unsurprisingly, the model shows very little temperature rise in the target and no target ablation for either titanium or iron. Yet the model still tells us something important about filaments, namely that the plasma column alone is not responsible for any of the filament-exclusive shapes discussed in the previous sections. Even by increasing the plasma duration to 100 ns, the target temperature change does not result in ablation. Thus, the effects of the ablation on the targets shown above are due to interaction with the initial laser pulse, not post-pulse interaction with the plasma column. The plasma column may have some affect on the filament–target interaction, but the modeling results discussed here indicate that that effect is not thermal or ablative in nature.

## 5 Conclusion

The filament's unique behavior to create an intense and narrowly diverging pulse of power with a plasma column over long distances remains an intriguing method to ablate solid materials. In contrast to using a short focal length lens, a filament can ablate and mark materials over a much longer distance (10–100 m). As evidenced by removing the focusing lens, we see nearly reproducible ablation characteristics over many meters though these are not as well defined as when a short focal length lens is used. The drawback of filament ablation is a smaller amount of material removed that could be of importance to an application like FIBS with the additional variables of focusing paradigm and substrate material. Using a short focal length lens is clearly superior if the goal is to perform a precise, well-defined cut with the highest rate of material

removal. Ablation with a filament shows promise when the target is at varying or far distances from the laser. However, the results shown here lead to further investigation into understanding how target material properties lead to substantial differences in results from filament ablation.

**Acknowledgements** The authors express their gratitude for the assistance at the U.S. Army Research Laboratory from Jeffrey Ball; Robert Borys, Jr.; Frank De Lucia, Jr.; Jennifer Gottfried; Gregory Gentle; and David MacKenzie. The authors also express their gratitude to Casey Boutwell, Ming Wei, and Matthieu Baudelet at the University of Central Florida. The authors also would like to acknowledge funding from the U.S. Army Research Laboratory and research at the University of Central Florida is funded under the JTO/AFOSR MRI on “Fundamentals of Filament Interaction” number FA95501110001 and The State of Florida.

## References

1. A. Couairon, A. Mysyrowicz, *Phys. Rep.* **441**, 47 (2007)
2. L. Bergé, S. Skupin, R. Nuter, J. Kasparian, J.-P. Wolf, *Rep. Prog. Phys.* **70**, 1633 (2007)
3. V.P. Kandidov, S.A. Shlenov, O.G. Kosareva, *Quant. Elec.* **39**, 205 (2009)
4. B. La Fontaine, F. Vidal, Z. Jiang, C.Y. Chien, D. Comtois, A. Desparois, T.W. Johnston, J.-C. Kieffer, H. Pépin, H.P. Mercure, *Phys. Plasmas* **6**, 1615 (1999)
5. A. Ting, I. Alexeev, D. Gordon, R. Fischer, D. Kaganovich, T. Jones, E. Briscoe, J. Peñano, R. Hubbard, P. Sprangle, *Phys. Plasmas* **12**, 056705 (2005)
6. H. Yang, Y. Li, J. Zhang, Y. Li, Z. Chen, H. Teng, Z. Wei, Z. Sheng, *Phys. Rev. E* **66**, 016406 (2002)
7. W. Liu, f. Théberge, E. Arévalo, J.-F. Gravel, A. Becker, S.L. Chin, *Opt. Lett.* **30**, 2602 (2005)
8. S. Tzortzakis, B. Prade, M. Franco, A. Mysyrowicz, *Opt. Commun.* **181**, 123 (2000)
9. J. Cheng, C.-S. Liu, S. Shang, D. Liu, W. Perrie, G. Dearden, K. Watkins, *Opt. Laser Tech.* **46**, 88 (2013)
10. B.N. Chichkov, C. Momma, S. Nolte, F. von Alvensleben, A. Tünnermann, *Appl. Phys. A* **63**, 109 (1996)
11. B. Rethfeld, K. Sokolowski-Tinten, D. von der Linde, S.I. Anisimov, *Phys. Rev. B* **65**, 092103 (2002)
12. J.K. Chen, W.P. Latham, J.E. Beraun, *J. Laser Appl.* **17**, 63 (2005)
13. D. Kiselev, L. Woeste, J.-P. Wolf, *Appl. Phys. B* **100**, 515 (2010)
14. M. Weidman, K. Lim, M. Ramme, M. Durand, M. Baudelet, M. Richardson, *Appl. Phys. Lett.* **101**, 034101 (2012)
15. M.R. Leahy-Hoppa, J. Miragliotta, R. Osiander, J. Burnett, Y. Dikmelik, C. McEnnis, J.B. Spicer, *Sensors* **10**, 4342 (2010)
16. D.W. Hahn, N. Omenetto, *Appl. Spectrosc.* **66**, 347 (2012)
17. Ph. Rohwetter, K. Stelmazczyk, L. Wöste, R. Ackermann, G. Méjean, E. Salmon, J. Kasparian, J. Yu, J.-P. Wolf, *Spectrochim. Acta B* **60**, 1025 (2005)
18. S. Tzortzakis, D. Anglos, D. Gray, *Opt. Lett.* **31**, 1139 (2006)
19. B. Zeng, T.-J. Wang, S. Hosseini, Y. Cheng, Z. Xu, W. Liu, S.L. Chin, *J. Opt. Soc. Am. B* **29**, 3226 (2012)
20. D. R. Lide, editor: *CRC Handbook of Chemistry and Physics*. (CRC Press, Boca Raton 1996)
21. J. A. Dean, Editor: *Lange's Handbook of Chemistry*. (McGraw-Hill, New York, NY 1999)
22. S. Juodkakis, H. Okuno, N. Kujime, S. Matsuo, H. Misawa, *Appl. Phys. A* **79**, 1555 (2004)

23. M.A. Ordal, J. Bell Robert, Jr. R.W. Alexander, L.L. Long, M.R. Query, *Appl. Opt.* **24**, 4493 (1985)
24. A.A. Ionin, S.I. Kudryashov, S.V. Makarov, L.V. Seleznev, D.V. Sinitsyn, *J. Euro. Theo. Phys. Lett.* **90**, 423 (2009)
25. G. Fibich, S. Eisenmann, B. Ilan, A. Zigler, *Opt. Lett.* **29**, 1772 (2004)
26. Kiran P. Prem, S. Bagchi, S.R. Krishnan, C.L. Arnold, G.R. Kumar, A. Couairon, *Phys. Rev. A* **82**, 013805 (2010)
27. W. Liu, S.L. Chin, *Opt. Express* **13**, 5750 (2005)
28. A.A. Ionin, S.I. Kudryashov, S.I. Kudryashov, S.V. Makarov, L.V. Seleznev, D.V. Sinitsyn, E.V. Golosov, O.A. Golosova, Y.R. Kolobov, A.E. Ligachev, *Appl. Phys. A* **107**, 301 (2012)
29. H. Tao, J. Lin, Z. Hao, X. Gao, X. Song, C. Sun, X. Tan, *Appl. Phys. Lett.* **100**, 201111 (2012)
30. A. J. Porwitzky, An End-To-End Model of an Electrothermal Chemical Gun. PhD thesis, University of Michigan Department of Aerospace Engineering (2008)
31. S.I. Anisimov, *J. Sov. Phys. JETP* **27**, 182 (1968)
32. A.J. Porwitzky, M. Keidar, I.D. Boyd, *IEEE Trans. Mag.* **43**, 313 (2007)